Elastic scattering of ^{7}Be + ^{28}Si at near-barrier energies

O. Sgouros,[1] A. Pakou,[1,*] D. Pierroutsakou,[2] M. Mazzocco,[3,4] L. Acosta,[5,6] X. Aslanoglou,[1] Ch. Betsou,[1] A. Boiano,[2] C. Boiano,[7] D. Carbone,[8] M. Cavallaro,[8] J. Grebosz,[9] N. Keeley,[10] M. La Commara,[2,11] C. Manea,[4] G. Marquínez-Durán,[12] I. Martel,[12] N. G. Nicolis,[1] C. Parascandolo,[2] K. Rusek,[13] A. M. Sánchez-Benítez,[12,14] C. Signorini,[15] F. Soramel,[3,4] V. Soukeras,[1] C. Stefanini,[3] E. Stiliaris,[16] E. Strano,[3,4] I. Strojek,[10] and D. Torresi[3,4]

[1]*Department of Physics and HINP, The University of Ioannina, 45110 Ioannina, Greece*
[2]*INFN, Sezione di Napoli, via Cintia, 80126 Napoli, Italy*
[3]*Dipartimento di Fisica e Astronomia, Università di Padova, via Marzolo 8, I-35131 Padova, Italy*
[4]*INFN, Sezione di Padova, via Marzolo 8, I-35131 Padova, Italy*
[5]*Instituto de Fisica, Universidad Nacional Autonoma de Mexico, Mexico D.F. 01000, Mexico*
[6]*INFN, Sezione di Catania, via Santa Sofia 64, 95125 Catania, Italy*
[7]*INFN, Sezione di Milano, via Celoria 16, I-20133 Milano, Italy*
[8]*INFN Laboratori Nazionali del Sud, via Santa Sofia 62, 95125 Catania, Italy*
[9]*The Henryk Niewodniczański Institute of Nuclear Physics (IFJ PAN), Kraków, Poland*
[10]*National Centre for Nuclear Research, ulica Andrzeja Sołtana 7, 05-400 Otwock, Poland*
[11]*Dipartimento di Scienze Fisiche, Università di Napoli "Federico II", via Cintia, I-80126 Napoli, Italy*
[12]*Departamento de Ciencias Integradas, Universidad de Huelva, E-21071 Huelva, Spain*
[13]*Heavy Ion Laboratory, University of Warsaw, Pasteura 5a, 02-093 Warsaw, Poland*
[14]*Centro de Física Nuclear da Universidade de Lisboa, 1649-003 Lisboa, Portugal*
[15]*INFN, LNL, viale dell'Università 2, I-35020 Legnaro, Italy*
[16]*Institute of Accelerating Systems and Applications and Department of Physics, University of Athens, Greece*

(Received 1 February 2017; published 11 May 2017)

The elastic scattering of the radioactive nucleus ^{7}Be from a ^{28}Si target was studied at four near-barrier energies: 13.2, 17.2, 19.8, and 22.0 MeV ($E/V_C = 1.14$, 1.48, 1.71, and 1.90). Angular distribution measurements were performed at each energy with the multidetector array EXPADES in conjunction with two Parallel-Plate Avalanche Counters (PPAC) to enable beam ray reconstruction of the events. The data are analyzed in a double-folding framework and the energy evolution of the optical potential as well as the total reaction cross sections are deduced and discussed.

DOI: 10.1103/PhysRevC.95.054609

I. INTRODUCTION

Interest in the interplay between elastic scattering and reaction mechanisms at energies close to the Coulomb barrier has been strong for many years now. A phenomenological optical model approach is often adopted to describe the elastic scattering. The optical model replaces the complex many-body problem of the interaction of two nuclei by the interaction of two structureless particles via an effective potential, with the effect of nonelastic processes, leading to absorption of flux out of the elastic channel, represented by the addition of an imaginary term to the potential. This picture may be improved by considering the interaction within the double-folding model framework [1], which provides a basis for describing heavy-ion scattering microscopically. In the double-folding model the nuclear matter densities of the two interacting nuclei are folded with an effective nucleon-nucleon interaction to obtain the real part of the nucleus-nucleus potential.

A first indication of unusual behavior by the effective potential in the vicinity of the Coulomb barrier was provided by optical model analyses of the ^{16}O + ^{208}Pb [2] and ^{32}S + ^{40}Ca [3] elastic scattering. A rapid and localized variation with incident energy of the surface strength of the optical potential was found as the Coulomb barrier was approached. This variation was manifest as a bell-shaped peak in the strength of the real part of the potential associated with a sharp decrease in the strength of the imaginary part, due to the closing of reaction channels as the barrier is approached and the consequent reduction in the amount of absorption out of the elastic channel. The term "threshold anomaly" (TA) [4] was subsequently applied to such cases and it was demonstrated that the behavior of the real part of the potential was linked to that of the imaginary part via a dispersion relation [5].

With the advent of radioactive beam (RIB) facilities interest switched to cases with weakly bound projectiles, stable as well as radioactive, where the influence of breakup effects and the importance of transfer reactions make the conditions more complicated. It was suggested [6–8] that since the polarization potential produced by breakup is repulsive in nature it could compensate for the attractive component of the real polarization potential generated by coupling to other direct channels (inelastic scattering to bound states and breakup) and responsible for the anomaly. It was therefore considered possible [6] that the dispersion relation might not apply to weakly bound systems, since according to theoretical calculations [7] the repulsive contribution of breakup to the real part of the potential is almost independent of beam energy

*Corresponding author: apakou@cc.uoi.gr

while the associated contribution to the imaginary part is small. Indeed the pioneering experimental work on the elastic scattering of the weakly bound but stable projectiles ^{6}Li and ^{7}Li on lead and barium targets [9,10] found unusual behavior for ^{6}Li but not for ^{7}Li, which appeared to show a conventional TA. It should be recalled that the breakup thresholds for ^{6}Li and ^{7}Li are 1.47 and 2.47 MeV, respectively. Later a new manifestation of the anomaly for ^{6}Li was observed in the ^{6}Li + ^{28}Si system [11] and interpreted in terms of dispersion relations [12]. With the aid of a reanalysis of previous data an increasing trend of the surface strength of the imaginary potential was observed for ^{6}Li but not for ^{7}Li [11,12], as the Coulomb barrier was approached from higher to lower energies. This behavior was related via dispersion relations with an almost flat evolution of the real part of the potential as a function of energy (with a shallow valley at the barrier), developing a bell-shaped peak at very low energies well below the barrier [12–15]. The new manifestation of the anomaly for ^{6}Li was discussed later in Ref. [16] and named the "breakup threshold anomaly." Currently the new anomaly is reasonably well established for ^{6}Li but not for ^{7}Li, although not fully understood, and verified in numerous articles for various targets such as ^{27}Al [17], ^{28}Si [11,12], ^{58}Ni [18], ^{59}Co [19], ^{64}Zn [20], ^{80}Se [21], ^{90}Zr [22], ^{112,116}Sn [23], ^{138}Ba [10], ^{144}Sm [24], ^{208}Pb [9], ^{209}Bi [25], and ^{232}Th [26]. A review of these measurements can be found in Ref. [27].

The situation is less clear for radioactive projectiles. Existing measurements are reviewed in Refs. [27–29] and mainly concern the neutron-rich nucleus ^{6}He and the proton-rich nuclei ^{8}B and ^{7}Be. Comprehensive work on the energy dependence of the potential via analysis of angular distribution measurements has been performed for ^{6}He incident on both ^{208}Pb [30,31] and ^{209}Bi [32] targets. The conclusion is that the behavior of the optical potential for ^{6}He is the same as that for ^{6}Li and may be attributed to the very low binding energy of the two neutrons to the α core of 0.973 MeV. Elastic scattering measurements with the cocktail radioactive beam (^{8}B, ^{7}Be,^{6}Li) of Notre Dame on ^{58}Ni are presented in Ref. [33] and the data are analyzed in terms of various optical potentials in Ref. [34]. The initial conclusion, although given with caution due to the large uncertainties assigned to the potential parameters, is that both proton-rich nuclei, ^{8}B and ^{7}Be, present the same trend as that for ^{6}Li, which was measured and analyzed simultaneously. This conclusion was later reconfirmed for ^{8}B in Ref. [35]. It was however reconsidered later for ^{7}Be, for which a comprehensive analysis combining fusion and elastic scattering data was subsequently performed [36]. The new evidence supports a similarity between ^{7}Be and its mirror nucleus ^{7}Li, both presenting the usual threshold anomaly. The most recent measurement of this type appearing in the literature for a radioactive projectile again concerns the proton-rich ^{7}Be nucleus and its elastic scattering from ^{27}Al [37]. The data were collected at two RIB facilities, situated at the University of São Paulo and the University of Notre Dame. Due to the low beam flux thick targets had to be used. Optical model analyses of the data are consistent with an energy-independent optical potential around the barrier but this conclusion is given as susceptible to the use of a very thick target. It is obvious from the above that for radioactive projectiles more experimental work is needed. Also taking into account that in principle the deduction of the optical potential at near-barrier energies is a difficult task even for stable projectiles, since the Coulomb interaction is dominant, other tools or reaction channels should be considered to help in obtaining firm conclusions. This is well illustrated in Refs. [13–15].

Within this spirit, we present here new elastic scattering data for ^{7}Be + ^{28}Si at near-barrier energies (E/V_C = 1.1 to 1.9). An optical model analysis is performed within the BDM3Y1 framework and the energy evolution of the optical model parameters is obtained. Data for the α production in this system were measured simultaneously and fusion and total reaction cross sections were deduced and reported in Ref. [38]. These results are considered together with the present elastic scattering data to obtain firmer conclusions. Continuum Discretized Coupled Channels (CDCC) calculations were also performed and are discussed in relation to the elastic scattering data.

This paper is organized as follows. Section II describes the experimental setup and Sec. III the data reduction procedure. The optical model analysis is included in Sec. IV, while the CDCC calculations are described in Sec. V. Finally, some concluding remarks and a summary of our results are given in Sec. VI.

II. EXPERIMENTAL DETAILS

The ^{7}Be secondary beam was produced at the EXOTIC facility [39–43] of the Laboratori Nazionali di Legnaro (LNL), Italy, by means of the in-flight technique and the ^{1}H(^{7}Li,^{7}Be)n reaction. This beam has been produced regularly at the EXOTIC facility for several years now and a comprehensive description of the beam is given in Ref. [44]. Details pertinent to this work are given below. The $^{7}Li^{3+}$ primary beam was delivered by the LNL-XTU Tandem Van de Graaff accelerator with an intensity of ∼150 pnA at energies of 26, 31, and 33 MeV. The primary beam was directed onto a 5-cm-long gas cell with 2.2-μm-thick Havar foil windows filled with H_2 gas at a pressure of ∼1000 mbar and a temperature of 93 K, corresponding to an effective thickness of 1.35 mg/cm^2. The ^{7}Be beam was produced at four energies: 13.2, 17.2, 19.8, and 22 MeV, the highest three being obtained by retuning the primary beam while the lowest was obtained using a degrader. The beam passed through two x-y sensitive parallel-plate avalanche counters (PPACs) located along the beam line 909 mm ($PPAC_A$) and 365 mm ($PPAC_B$) [45] upstream of the secondary target then impinged with a flux of $\sim 5 \times 10^4$ pps on a 0.4-mg/cm^2-thick ^{28}Si target (0.6 mg/cm^2 for the 17.2 MeV data). Both the elastically scattered ^{7}Be nuclei and the reaction products were recorded in EXPADES [45,46], the detector array of the EXOTIC facility. The experimental setup, a schematic view of which is presented in Fig. 1, included six telescopes from EXPADES. Each telescope comprised ΔE and E double-sided silicon strip detectors (DSSSD) with thicknesses of ∼55 and 300 μm, respectively. Both modules had active areas of 64×64 mm^2 with 32 strips per side, orthogonally oriented to define 2×2 mm^2 pixels. Details of how the detector signals were handled can be found in Ref. [45].

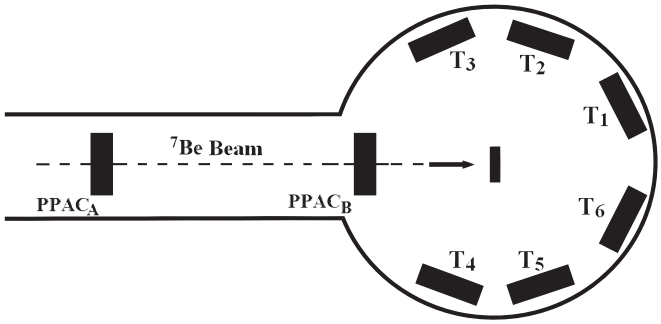

FIG. 1. Schematic view of the experimental setup which includes six of the eight modules of the EXPADES array [45,46]. Each module-telescope comprises two DSSSD detectors as explained in the text. Telescopes T1 and T6 were set at ±27°, T2 and T5 at ±69°, and T3 and T4 at ±111°, spanning the following angular ranges: ∼13° to 41° and ∼14° to 40° for the forward detectors, ∼54° to 85° for the middle telescopes, and ∼96° to 126° for the backward telescopes.

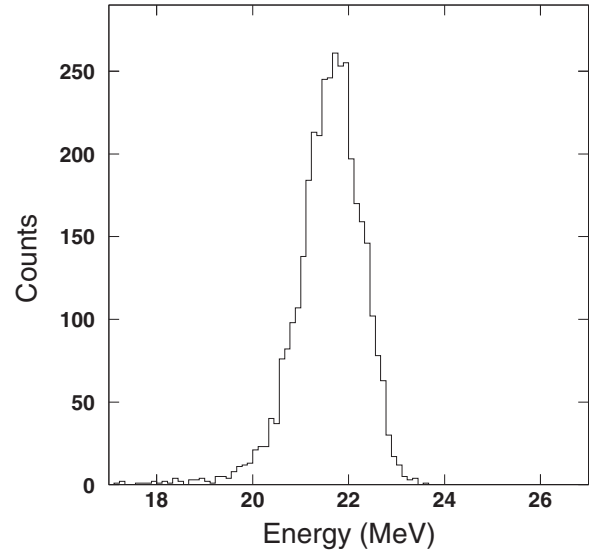

FIG. 2. An energy spectrum for elastic scattering of ^{7}Be + ^{28}Si at 22 MeV and $\theta_{lab} = 17.5°$, collected by one strip of detector T6 (see Fig. 1).

The strips were short-circuited two-by-two, therefore the angular resolution was in principle ∼2° per angular position, considering a pointlike beam spot on target. The forward telescopes T1 and T6 were set at ±27°, T2 and T5 at ±69°, and T3 and T4 at ±111°, spanning the following angular ranges: ∼13° to 41° and ∼14° to 40° for the forward telescopes, ∼54° to 85° for the middle telescopes, and ∼96° to 126° for the backward telescopes. The telescopes were set at symmetrical positions to balance any beam divergence and to improve the statistics of the measurement. The trigger of the electronics was given by a signal created by the OR of the ΔE stage of the telescopes in coincidence with the PPAC signal set. The reaction products, ^{3}He and ^{4}He, were well separated by the ΔE-E technique and their analysis was reported previously in Ref. [38]. The elastically scattered ^{7}Be events were stopped in the first stage of the telescopes. The energy loss of the light reaction products accumulated in these detectors while passing through was small in comparison with the dissipated energy of the elastically scattered ^{7}Be nuclei. Therefore the peaks corresponding to ^{7}Be events were clearly separated as it can be seen in Fig. 2. The energy resolution of the peaks was ∼1.5 MeV, which did not allow the separation of inelastic events; therefore the present results actually represent quasielastic scattering. However, test calculations suggest that the inelastic scattering contribution is small, within the experimental uncertainties, so that the data may be taken as pure elastic for all practical purposes.

III. DATA REDUCTION

The elastically scattered ^{7}Be nuclei were considered in an event-by-event analysis using the two PPAC signals to enable reconstruction of the beam ray and elastic scattering trajectories. The positions of the reaction vertex on the target and of the DSSSD x-y strip struck by the elastically scattered nucleus were thus unambiguously defined for each event, leading to a more precise assignment of angle. Events with the same angle or with an angle inside an angular range corresponding to the dimensions of a particular strip of each EXPADES detector ($\Delta\theta \sim 2°$) were summed up and were appropriately normalized for the deduction of differential cross sections. Solid angles were defined in a separate experiment with a lead target, where the scattering was Rutherford at all angles and the cross section therefore well known. The event-by-event analysis improved greatly over our preliminary strip and/or pixel analysis reported previously [47]. Differential cross sections were deduced according to the relation

$$\sigma/\sigma_{\text{Ruth-silicon}} = \frac{N_{\text{silicon}}}{N_{\text{lead}}} * K, \tag{1}$$

where N_{silicon} and N_{lead} are the event-by-event counts corresponding to the angular range subtended by each strip collected with the silicon and lead targets, respectively. The constant K corresponds to

$$K = \frac{\Phi_{\text{lead}} S_{\text{lead}} \sigma_{\text{Ruth-lead}}}{\Phi_{\text{silicon}} S_{\text{silicon}} \sigma_{\text{Ruth-silicon}}}, \tag{2}$$

where Φ_{silicon} and Φ_{lead} are the beam fluxes during the experiments with the silicon and lead targets, respectively; S_{silicon} and S_{lead} are the scattering centers of the silicon and lead targets, respectively; and $\sigma_{\text{Ruth-lead}}$ and $\sigma_{\text{Ruth-silicon}}$ are the Rutherford cross sections for ^{7}Be scattered by ^{2}08Pb and ^{2}8Si, respectively. The constant K was obtained by restricting the ratio $\sigma/\sigma_{\text{Ruth}}$ to ∼1 for data at forward angles where the scattering is Rutherford. Our differential cross sections are thus independent of uncertainties in beam flux, target thickness, and solid angle, and the error bars on the measured angular distributions are dominated by the statistical uncertainties of the measurements with the silicon and lead targets. The differential cross sections thus obtained for ^{7}Be incident energies of 13.2, 17.2, 19.8, and 22 MeV are presented in Figs. 3, 4, 5, and 6, respectively.

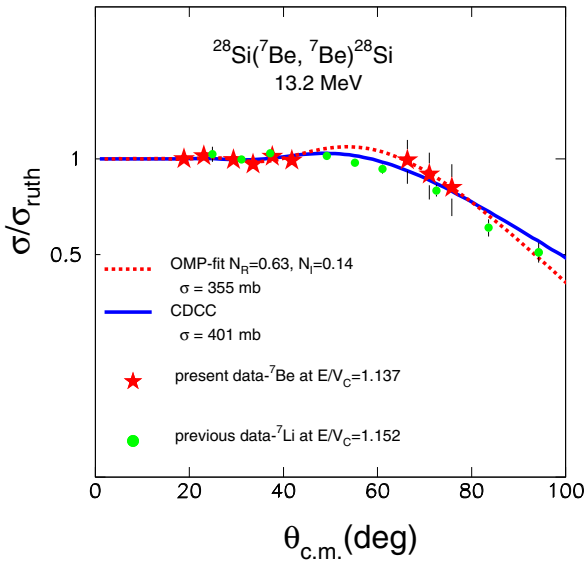

FIG. 3. Angular distribution for the elastic scattering of ^{7}Be + ^{28}Si at 13.2 MeV ($E/V_C = 1.137$), denoted by the red stars, compared with previous data [12] for ^{7}Li + ^{28}Si at 10 MeV ($E/V_C = 1.152$), denoted by the green circles. The dot-dashed red line denotes the best-fit OMP calculation while the solid blue line denotes the result of a CDCC calculation.

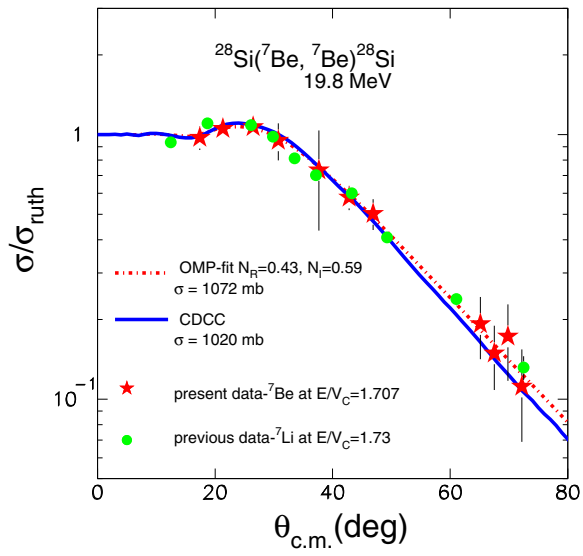

FIG. 5. Angular distribution for the elastic scattering of ^{7}Be + ^{28}Si at 19.8 MeV ($E/V_C = 1.707$), denoted by the red stars, compared with previous data [12] for ^{7}Li + ^{28}Si at 15 MeV ($E/V_C = 1.73$), denoted by the green circles. The dot-dashed red line denotes the best-fit OMP calculation while the solid blue line denotes the result of a CDCC calculation.

IV. OPTICAL MODEL ANALYSIS

We used the same method as that adopted previously for the ^{6,7}Li + ^{28}Si systems [11,12], and the elastic scattering calculations were performed with the code ECIS [48]. The real part of the optical model potential (OMP) was calculated using the double-folding model [1] with the BDM3Y1 interaction developed by Khoa *et al.* [49]. The nuclear matter densities required were obtained from electron scattering data for ^{28}Si [50], suitably corrected to derive a matter density from the empirical charge density [1], and a semiphenomenological analytic expression taking into account the asymptotic behavior

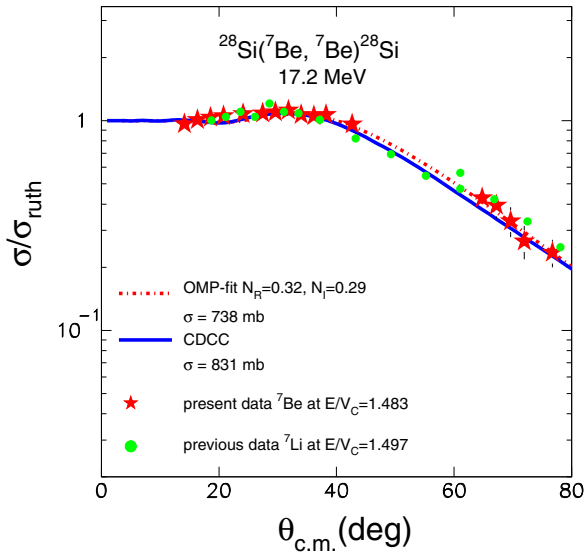

FIG. 4. Angular distribution for the elastic scattering of ^{7}Be + ^{28}Si at 17.2 MeV ($E/V_C = 1.483$), denoted by the red stars, compared with previous data [12] for ^{7}Li + ^{28}Si at 13 MeV ($E/V_C = 1.497$), denoted by the green circles. The dot-dashed red line denotes the best-fit OMP calculation while the solid blue line denotes the result of a CDCC calculation.

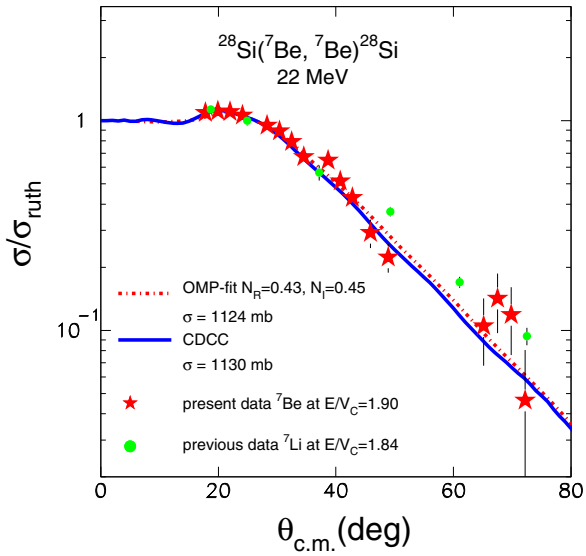

FIG. 6. Angular distribution for the elastic scattering of ^{7}Be + ^{28}Si at 22 MeV ($E/V_C = 1.90$), denoted by the red stars, compared with previous data [12] for ^{7}Li + ^{28}Si at 16 MeV ($E/V_C = 1.84$), denoted by the green circles. The dot-dashed red line describes the best-fit OMP calculation while the solid blue line denotes the result of a CDCC calculation.

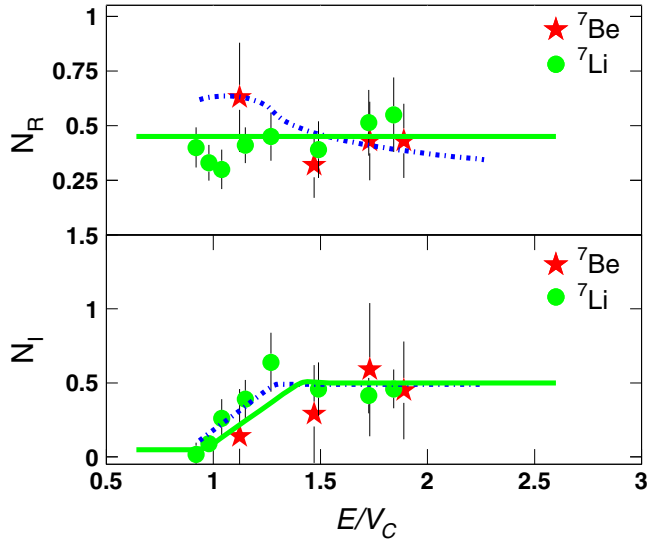

FIG. 7. The energy evolution of the optical model parameters: N_R and N_I, obtained in a BDM3Y1 framework (see text) for ^{7}Be + ^{28}Si, denoted by the red stars, compared with the optical model parameters for ^{7}Li + ^{28}Si [12], denoted by the green circles. The dot-dashed line corresponds to a dispersion relation analysis for ^{7}Li performed previously [12]. See text for an explanation of the solid green line.

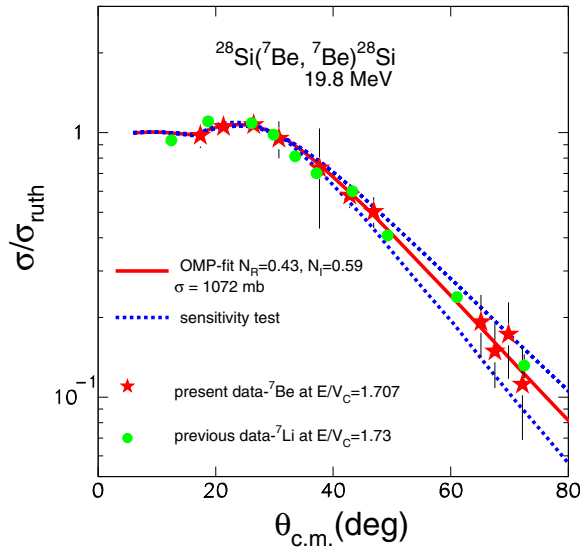

FIG. 8. Sensitivity analysis for the elastic scattering data at 19.8 MeV.

and the behavior of the density at the nuclear center [51] for ^{7}Be.

The imaginary potential was assumed to be of the same radial shape as the real one, the same folded potential being adopted but with a different normalization factor. A search was performed with the normalization factors of the real and imaginary potentials, N_R and N_I, as free parameters. The best-fit values of N_R and N_I are plotted in Fig. 7, while the corresponding angular distributions are compared with the data in Figs. 3, 4, 5, and 6. The uncertainties in the potential parameters plotted in Fig. 7 were deduced from a sensitivity analysis performed by varying the parameters N_R and N_I by prescribed amounts. A representative plot of the sensitivity analysis is shown in Fig. 8 for the 19.8 MeV data. We consider it more appropriate to plot rather these normalization factors [11] as a function of energy than the values of the real and imaginary potentials at the strong absorption radius, since for light elements the radial region of sensitivity may change significantly with bombarding energy. The definition of the strong absorption radius is not straightforward for weakly bound encounters, as was pointed out in Refs. [52,53]. Moreover in Ref. [11] an analysis adopting a Woods-Saxon form for the imaginary part of the optical potential gave the same results as one using the same folding interaction as for the real part, thus reinforcing the present analysis methodology. By adjusting only two parameters we also reduce the potential ambiguities as much as possible, within the constraints of data obtained with the limited intensities available for RIBs.

The energy evolution of the optical potential parameters is displayed in Fig. 7. Due to the large errors we cannot draw firm conclusions solely from the elastic scattering data. We may only discuss the overall trend of these data, which seems to be compatible with a standard threshold anomaly, at least in what concerns the imaginary part, with a decreasing magnitude as we approach the barrier from higher to lower energies. However, the agreement of the present data with the dispersion relation cannot be confirmed because in the critical energy region, where a peak should appear in the real potential, we possess only one datum. In the same figure we present previous results for ^{7}Li on the same target, ^{28}Si, originating from two separate experiments: an elastic scattering angular distribution measurement [12] (designated by the green dots) and a barrier distribution measurement [14] (designated by the solid green lines). If we assume the energy dependence of N_I to be that designated by the dot-dashed blue line in the lower panel of Fig. 7 the dispersion relation predicts the behavior of N_R as a function of energy given by the dot-dashed blue curve in the upper panel. By comparing all the information included in this figure from both the elastic scattering and barrier distribution experiments we can in principle conclude that the optical potentials for the mirror nuclei ^{7}Li and ^{7}Be present a similar energy dependence. The decreasing imaginary potentials follow the behavior of the standard threshold anomaly but the dispersion relation does not hold for ^{7}Li [14] and possibly not for ^{7}Be (the uncertainties for ^{7}Be are such that the existence of the peak in N_R predicted by the dispersion relation cannot be verified). This evidence, if combined with the results for the α-production data collected in the same experiment and reported in Ref. [38], indicates with some confidence a similarity of the two mirror nuclei. In Ref. [38] the fusion hindrance of both ^{7}Li and ^{7}Be compared to ^{6}Li was reported and the similarity between the two mirror nuclei was suggested.

The optical model analysis also yields total reaction cross sections, which are included in Table I. The assigned errors come from the sensitivity analysis performed for the normalization factors N_R and N_I. In the same table we have

TABLE I. Total reaction cross sections for ^{7}Be + ^{2}8Si obtained in the present experiment via an optical model analysis, σ_{elast}, are compared with previous values deduced in an α-production experiment [38], $\sigma_{\alpha-\text{production}}$, as well as with a phenomenological prediction [54], σ_{pred}, and theoretical values extracted from our CDCC calculations, σ_{CDCC}. The first column gives the projectile incident energies at the front of the target, E_{lab}, while the second column gives the reaction energy in the middle of the target, E_{rea}.

E_{lab} (MeV)	E_{rea} (MeV)	σ_{elast} (mb)	$\sigma_{\alpha\text{-production}}$ (mb)	σ_{pred} (mb)	σ_{CDCC} (mb)
22	21.7	1124 ± 148	1232 ± 195	1118	1130
19.8	19.5	1072 ± 163	1126 ± 242	990	1020
17.2	16.7	738 ± 190	—	779	831
13.2	12.9	355 ± 95	258 ± 63	347	401

also included the total reaction cross sections obtained in our previous work on the α-particle production in the ^{7}Be + ^{28}Si system and those obtained with the phenomenological prediction as deduced for light targets in Ref. [54]. All results are found to be in very good agreement, supporting our present optical model analysis. The present results are compared with previous results for weakly bound stable and radioactive projectiles on a similar (^{27}Al) or the same (^{28}Si) target in Fig. 9. The total reaction cross sections were reduced to total reaction cross-section functions, F_{TR}, as a function of the quantity x according to Refs. [55,56]. To avoid the problems underlined in Ref. [57] the comparison was restricted to light targets only. The definitions of F_{TR} and x are

$$\sigma_{\text{TR}} \rightarrow F_{\text{TR}}(x) = \frac{2E_{\text{c.m.}}}{\hbar\omega R_{\text{B}}^2}\sigma_{\text{TR}}, \tag{3}$$

corresponding to an energy in the center of mass, $E_{\text{c.m}}$, reduced to the quantity x given by the equation

$$E_{\text{c.m.}} \rightarrow x = \frac{E_{\text{c.m.}} - V_{\text{B}}}{\hbar\omega}. \tag{4}$$

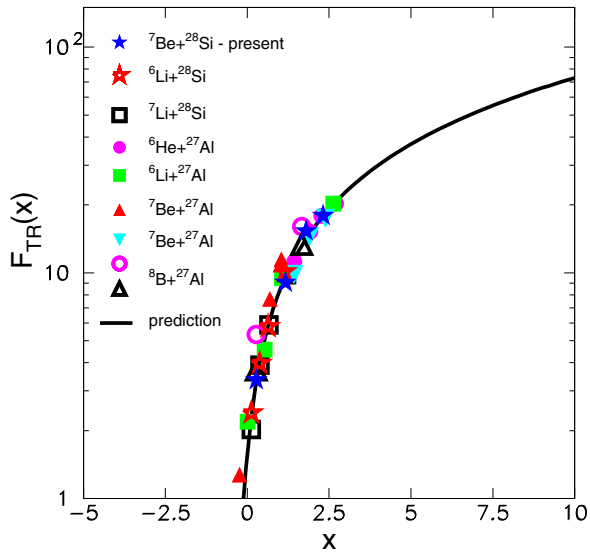

FIG. 9. Reduced total reaction cross sections for weakly bound projectiles on light targets. Previous data from Refs. [37,59–63] are compared with the present data and the prediction from Ref. [54] for light targets, denoted by the solid black line.

Curvatures ($\hbar\omega$), radii (R_{B}), and potential heights (V_{B}) were deduced using the Christensen-Winther potential [58]. As can be seen from Fig. 9, the present results show very good compatibility with previous data: ^{6,7}Li + ^{28}Si [59], ^{6}He + ^{27}Al [60], ^{6}Li + ^{27}Al [61], ^{7}Be + ^{27}Al [37,62], and ^{8}B + ^{27}Al [63]. It should be noted that the first set of ^{7}Be + ^{27}Al data [37] present total reaction cross sections larger than the second set [62], the present values, and all other data with other projectiles. The authors also give two experimental values for the cross section extracted from their optical model analysis for ^{8}B, either with the São Paulo potential (designated in Fig. 9 by the open black triangles) or with a Woods-Saxon one (designated in Fig. 9 by the open circles). In the same figure the prediction obtained in Ref. [54] is also included and describes the data very well.

V. CDCC CALCULATIONS

These calculations were performed using version FRXP.18 of the code FRESCO [64] for the system ^{7}Be + ^{28}Si in the energy range E_{lab} = 13.2 to 22 MeV (1.14 to 1.9 × V_C). The model used was similar to that of Ref. [65]. It was assumed that the ^{7}Be nucleus has a two-body ^{4}He + ^{3}He cluster structure. Couplings between resonant and nonresonant cluster states corresponding to ^{4}He + ^{3}He relative orbital angular momenta L = 0, 1, 2, 3, and 4 $\hbar$ were included. Excitation of the first-excited state and the ground-state reorientation were also taken into account. The continuum above the ^{7}Be → ^{4}He + ^{3}He breakup threshold was discretized into momentum bins. The upper limit of the continuum excitation energy was 9.4 MeV for the 19.8 and 22 MeV data and 7.7 MeV for the 17.2 and 13.2 MeV data. Tests with higher excitation energies and higher angular momenta did not change the results. The widths of the bins were set to $\Delta k = 0.23$ fm^{-1} for the 13.2 MeV data and $\Delta k = 0.20$ fm^{-1} for the other incident energies. In the presence of the resonant states the binning schemes were suitably modified to avoid double counting. All the diagonal and coupling potentials were generated from empirical α + ^{28}Si and ^{3}He + ^{28}Si optical model potentials by means of the single-folding technique. These potentials were taken from Refs. [66,67].

The elastic scattering angular distributions from the CDCC calculations are compared with the data in Figs. 3, 4, 5, and 6. Calculations for one-channel (^{7}Be ground-state reorientation only), two-channel (^{7}Be ground-state reorientation and excitation of the first-excited state), and full CDCC calculations are

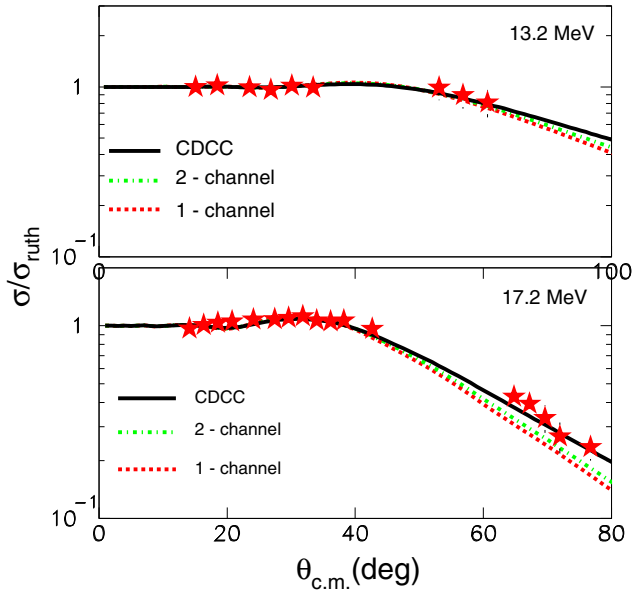

FIG. 10. Elastic scattering data for ^{7}Be + ^{28}Si at 13.2 MeV (top panel) and 17.2 MeV (bottom panel) compared with one-channel, two-channel, and CDCC calculations.

compared with the data in Fig. 10 for 13.2 and 17.2 MeV and Fig. 11 for 19.8 and 22 MeV. The agreement of the CDCC calculations with the data is very good, while it is obvious that couplings to ground-state reorientation and excitation of the first-excited state of ^{7}Be are unimportant and coupling to the continuum has the main influence on the elastic scattering, although it is still not very strong. Our CDCC calculations give low breakup cross sections of 13.4, 10.6, 7.4, and 3.4 mb for the 22, 19.8, 17.2, and 13.2 MeV data, respectively.

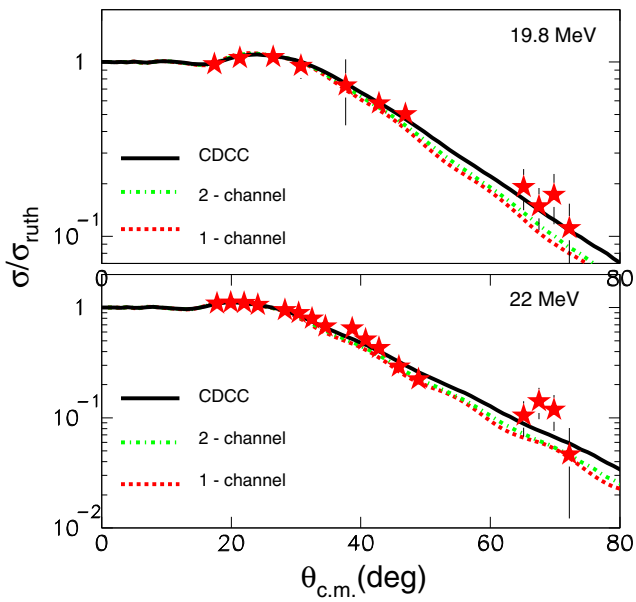

FIG. 11. Elastic scattering data for ^{7}Be + ^{28}Si at 19.8 MeV (top panel) and 22 MeV (bottom panel) compared with one-channel, two-channel, and CDCC calculations.

VI. DISCUSSION AND SUMMARY

We have performed measurements of the ^{7}Be + ^{28}Si elastic scattering at several near-barrier energies: 13.2, 17.2, 19.8, and 22 MeV ($E/V_C = 1.14$ to 1.9). The results were analyzed within the optical model framework using the double-folding model employing the BDM3Y1 interaction, and the energy evolution of the strengths of the real and imaginary parts of the optical potential was deduced. The large uncertainties prevent definite conclusions from being drawn based solely on the analysis of the elastic scattering angular distributions. The trend is consistent with a standard threshold anomaly behavior for this system, with a decreasing trend of the imaginary part around the barrier, although the existence of the corresponding peak in the real part cannot be confirmed. This is in accordance with the findings of a reanalysis of ^{7}Be + ^{58}Ni elastic scattering and fusion data [36].

Previous data for the ^{7}Li + ^{28}Si system were also considered in the same theoretical framework to draw meaningful comparisons concerning the similarity or otherwise of the two mirror nuclei. While the large uncertainties of the present measurement make the results in principle seem inconclusive, when combined with the fusion data reported in Ref. [38] they suggest with a certain confidence similarity between the two mirror nuclei.

We also obtained total reaction cross sections from the optical model analysis, which were found to be in very good agreement with previous measurements for the same system obtained via α-production measurements and global phenomenological predictions. Because total reaction cross sections are traditionally used to restrict the imaginary part of the optical potential, this compatibility further supports our result for the energy dependence of the potential. This raises questions concerning the dependence of threshold anomalylike behavior on the breakup threshold since ^{7}Be has a breakup threshold of 1.59 MeV, similar to that of ^{6}Li (1.47 MeV) rather than that of ^{7}Li (2.47 MeV), although the energy dependence of its optical potential seems to resemble rather its mirror nucleus ^{7}Li and not ^{6}Li. The total reaction cross sections obtained were also considered in a systematic framework and were found to be in very good agreement with those for other weakly-bound projectiles, stable as well as radioactive, incident on similar targets.

Finally, we performed CDCC calculations and compared these to the elastic scattering angular distribution data. It was found that the effect of coupling to the ground-state reorientation and excitation of the first-excited state of ^{7}Be is weak for this target and that while the breakup cross sections are small the effect of coupling to the continuum is significant in comparison but still not very strong.

In summary, the energy evolution of the optical potential for the ^{7}Be + ^{28}Si system at near-barrier energies was investigated. The trend of the results, together with previous total reaction cross section and fusion cross section measurements and corresponding data for the mirror nucleus ^{7}Li on the same target, indicate a possible similarity between the two mirror

nuclei and are consistent with the presence of a standard threshold anomaly (TA) for ^{7}Be, although this cannot be confirmed. Because the uncertainties for data taken with radioactive beams, especially when incident on low-mass targets, are large, more data for such systems are necessary to draw more systematic conclusions.

ACKNOWLEDGMENTS

This research was partially funded by the European Union Seventh Framework Programme FP7/2007-2013 under Grant No. 262010-ENSAR.

[1] G. R. Satchler and W. G. Love, Phys. Rep. **55**, 183 (1979).
[2] J. S. Lilley, B. R. Fulton, M. A. Nagarajan, I. J. Thompson, and D. W. Banes, Phys. Lett. B **151**, 181 (1985).
[3] A. Baeza, B. Bilwes, R. Bilwes, J. Diaz, and J. L. Ferrero, Nucl. Phys. A **419**, 412 (1984).
[4] G. R. Satchler, Phys. Rep. **199**, 147 (1991).
[5] M. A. Nagarajan, C. C. Mahaux, and G. R. Satchler, Phys. Rev. Lett. **54**, 1136 (1985).
[6] C. Mahaux, H. Ngo, and G. R. Satchler, Nucl. Phys. A **449**, 354 (1986).
[7] Y. Sakuragi *et al.*, Prog. Theor. Phys. **68**, 322 (1982).
[8] Y. Sakuragi *et al.*, Prog. Theor. Phys. **70**, 1047 (1983).
[9] N. Keeley *et al.*, Nucl. Phys. A **571**, 326 (1994).
[10] A. M. M. Maciel *et al.*, Phys. Rev. C **59**, 2103 (1999).
[11] A. Pakou, N. Alamanos, A. Lagoyannis *et al.*, Phys. Lett. B **556**, 21 (2003).
[12] A. Pakou, N. Alamanos, G. Doukelis *et al.*, Phys. Rev. C **69**, 054602 (2004).
[13] K. Zerva, N. Patronis, A. Pakou *et al.*, Phys. Rev. C **80**, 017601 (2009).
[14] K. Zerva, A. Pakou, N. Patronis *et al.*, Eur. Phys. J. A **48**, 102 (2012).
[15] K. Zerva, A. Pakou, K. Rusek *et al.*, Phys. Rev. C **82**, 044607 (2010).
[16] M. S. Hussein, P. R. S. Gomes, J. Lubian, and L. C. Chamon, Phys. Rev. C **73**, 044610 (2006); **76**, 019902(E) (2007).
[17] J. M. Figueira, D. Abriola, J. O. Fernandez Niello *et al.*, Phys. Rev. C **73**, 054603 (2006).
[18] M. Biswas, Subinit Roy, M. Sinha *et al.*, Nucl. Phys. A **802**, 67 (2008).
[19] F. A. Souza, L. A. S. Leal, N. Carlin, M. G. Munhoz, R. L. Neto, M. M. de Moura, A. A. P. Suaide, E. M. Szanto, A. Szanto de Toledo, and J. Takahashi, Phys. Rev. C **75**, 044601 (2007); **76**, 029901(E) (2007).
[20] M. Zadro, P. Figuera, A. Di Pietro *et al.*, Phys. Rev. C **80**, 064610 (2009).
[21] L. Fimiani, J. M. Figueira, G. V. Marti *et al.*, Phys. Rev. C **86**, 044607 (2012).
[22] H. Kumawat, V. Jha, B. J. Roy *et al.*, Phys. Rev. C **78**, 044617 (2008).
[23] N. N. Deshmukh, S. Mukherjee, D. Patel *et al.*, Phys. Rev. C **83**, 024607 (2011).
[24] J. M. Figueira, J. O. Fernandez Niello, A. Arazi *et al.*, Phys. Rev. C **81**, 024613 (2010).
[25] S. Santra, S. Kailas, K. Ramachandran, V. V. Parkar, V. Jha, B. J. Roy, and P. Shukla, Phys. Rev. C **83**, 034616 (2011).
[26] S. Dubey, S. Mukherjee, D. C. Biswas *et al.*, Phys. Rev. C **89**, 014610 (2014).
[27] L. F. Canto, P. R. S. Gomes, R. Donangelo, J. Lubian, and M. S. Hussein, Phys. Rep. **596**, 1 (2015).
[28] J. J. Kolata, V. Guimarães, and E. F. Aguilera, Eur. Phys. J. A **52**, 123 (2016).
[29] N. Keeley, N. Alamanos, K. W. Kemper, and K. Rusek, Prog. Part. Nucl. Phys. **63**, 396 (2009).
[30] A. M. Sanchez-Benitez, D. Escrig, M. A. G. Alvarez *et al.*, Nucl. Phys. A **803**, 30 (2008).
[31] L. Acosta, A. M. Sanchez-Benitez, M. E. Gomez *et al.*, Phys. Rev. C **84**, 044604 (2011).
[32] A. R. Garcia, J. Lubian, I. Padron *et al.*, Phys. Rev. C **76**, 067603 (2007).
[33] E. F. Aguilera, E. Martinez-Quiroz, D. Lizcano *et al.*, Phys. Rev. C **79**, 021601(R) (2009).
[34] A. G. Camacho, E. F. Aguilera, E. M. Quiroz *et al.*, Nucl. Phys. A **833**, 156 (2010).
[35] A. G. Camacho, E. F. Aguilera, P. R. S. Gomes, and J. Lubian, Phys. Rev. C **84**, 034615 (2011).
[36] A. G. Camacho and E. F. Aguilera, Phys. Rev. C **90**, 064607 (2014).
[37] V. Morcelle, R. Lichtenthaler, R. Linares *et al.*, Phys. Rev. C **89**, 044611 (2014).
[38] O. Sgouros, A. Pakou, D. Pierroutsakou *et al.*, Phys. Rev. C **94**, 044623 (2016).
[39] V. Z. Maidikov, T. Glodariu, M. La Commara *et al.*, Nucl. Phys. A **746**, 389c (2004).
[40] D. Pierroutsakou, B. Martin, T. Glodariu *et al.*, Eur. Phys. J.: Spec. Top. **150**, 47 (2007).
[41] F. Farinon, T. Glodariu, M. Mazzocco *et al.*, Nucl. Instrum. Methods Phys. Res., Sect. B **266**, 4097 (2008).
[42] M. Mazzocco, F. Farinon, T. Glodariu *et al.*, Nucl. Instrum. Methods Phys. Res., Sect. B **266**, 4665 (2008).
[43] M. Mazzocco, D. Torresi, E. Strano *et al.*, Nucl. Instrum. Methods Phys. Res., Sect. B **317**, 223 (2013).
[44] M. Mazzocco, D. Torresi, D. Pierroutsakou *et al.*, Phys. Rev. C **92**, 024615 (2015).
[45] D. Pierroutsakou, A. Boiano, C. Boiano *et al.*, Nucl. Instrum. Methods Phys. Res., Sect. A **834**, 46 (2016).
[46] E. Strano, A. Anastasio, M. Bettini *et al.*, Nucl. Instrum. Methods Phys. Res., Sect. B **317**, 657 (2013).
[47] O. Sgouros, A. Pakou, D. Pierroutsakou *et al.*, AIP Conf. Proc. **1645**, 397 (2015); INFN-LNL Report 241 (2015), p. 54.
[48] J. Raynal, Phys. Rev. C **23**, 2571 (1981).
[49] D. T. Khoa *et al.*, Phys. Lett. B **342**, 6 (1995).
[50] H. D. De Vries, C. W. Jager, and C. De Vries, At. Data Nucl. Data Tables **14**, 479 (1974).
[51] A. Bhagwat, Y. K. Gambhir, and S. H. Patil, Eur. Phys. J. A **8**, 511 (2000).
[52] D. Roubos, A. Pakou, N. Alamanos, and K. Rusek, Phys. Rev. C **73**, 051603(R) (2006).
[53] B. T. Kim, W. Y. So, S. W. Hong, and T. Udagawa, Phys. Rev. C **65**, 044607 (2002); **65**, 044616 (2002).

[54] A. Pakou, D. Pierroutsakou, M. Mazzocco *et al.*, Eur. Phys. J. A **51**, 55 (2015).
[55] L. F. Canto, P. R. S. Gomes, J. Lubian, L. C. Chamon, and E. Crema, J. Phys. G **36**, 015109 (2009).
[56] J. M. B. Shorto, P. R. S. Gomes, J. Lubian, L. F. Canto, S. Mukherjee, and L. C. Chamon, Phys. Lett. B **678**, 77 (2009).
[57] L. F. Canto, D. R. M. Junior, P. R. S. Gomes, and J. Lubian, Phys. Rev. C **92**, 014626 (2015).
[58] P. R. Christensen and A. Winther, Phys. Lett. B **65**, 19 (1976).
[59] A. Pakou, K. Rusek, N. Alamanos *et al.*, Eur. Phys. J. A **39**, 187 (2009).
[60] E. A. Benjamim, A. Lepine-Szily, D. R. M. Junior *et al.*, Phys. Lett. B **647**, 30 (2007).
[61] J. M. Figueira, J. O. F. Niello, D. Abriola *et al.*, Phys. Rev. C **75**, 017602 (2007).
[62] K. Kalita, S. Verma, R. Singh *et al.*, Phys. Rev. C **73**, 024609 (2006).
[63] V. Morcelle, R. Lichtenthaler, A. Lepine-Szily *et al.*, Phys. Rev. C **95**, 014615 (2017).
[64] I. J. Thompson, Comput. Phys. Rep. **7**, 167 (1988).
[65] N. Keeley, K. W. Kemper, and K. Rusek, Phys. Rev. C **66**, 044605 (2002).
[66] W. Wuhr, A. Hofmann, and G. Philipp, Z. Phys. **269**, 365 (1974).
[67] B. H. Wildenthal and P. W. M. Glaudemans, Nucl. Phys. A **92**, 353 (1967).